ELSEVIER

Journal of Quantitative Spectroscopy & Radiative Transfer 85 (2004) 337–365

Journal of Quantitative Spectroscopy & Radiative Transfer

www.elsevier.com/locate/jqsrt

Errors resulting from assuming opaque Lambertian clouds in TOMS ozone retrieval

X. Liu[a], M.J. Newchurch[a,*], R. Loughman[b], P.K. Bhartia[c]

[a] *Atmospheric Science Department, University of Alabama in Huntsville, 320 Sparkman Drive, Huntsville, AL 35805, USA*

[b] *Cooperative Center for Atmospheric Science and Technology, University of Arizona, Tucson, AZ 85721, USA*

[c] *Atmospheric Chemistry and Dynamics Branch, NASA Goddard Space Flight Center, Greenbelt, MD 20771, USA*

Received 23 January 2003; accepted 15 May 2003

Abstract

Accurate remote sensing retrieval of atmospheric constituents over cloudy areas is very challenging because of insufficient knowledge of cloud parameters. Cloud treatments are highly idealized in most retrieval algorithms. Using a radiative transfer model treating clouds as scattering media, we investigate the effects of assuming opaque Lambertian clouds and employing a Partial Cloud Model (PCM) on Total Ozone Mapping Spectrometer (TOMS) ozone retrievals, especially for tropical high-reflectivity clouds. Assuming angularly independent cloud reflection is good because the Ozone Retrieval Errors (OREs) are within 1.5% of the total ozone (i.e., within TOMS retrieval precision) when Cloud Optical Depth (COD) $\geqslant 20$. Because of Intra-Cloud Ozone Absorption ENhancement (ICOAEN), assuming opaque clouds can introduce large OREs even for optically thick clouds. For a water cloud of COD 40 spanning 2–12 km with 20.8 Dobson Unit (DU) ozone homogeneously distributed in the cloud, the ORE is 17.8 DU in the nadir view. The ICOAEN effect depends greatly on solar zenith angle, view zenith angle, and intra-cloud ozone amount and distribution. The TOMS PCM is good because negative errors from the cloud fraction being underestimated partly cancel other positive errors. At COD $\leqslant 5$, the TOMS algorithm retrieves approximately the correct total ozone because of compensating errors. With increasing COD up to 20–40, the overall positive ORE increases and is finally dominated by the ICOAEN effect. The ICOAEN effect is typically 5–13 DU on average over the Atlantic and Africa and 1–7 DU over the Pacific for tropical high-altitude (cloud top pressure $\leqslant 300$ hPa) and high-reflectivity (reflectivity $\geqslant 80\%$) clouds. Knowledge of TOMS ozone retrieval errors has important implications for remote sensing of ozone/trace gases from other satellite instruments.

Keywords: Ozone retrieval; TOMS; Cloud; Opaque Lambertian clouds

* Corresponding author. Tel.: +1-256-961-7825; fax: +1-256-961-7751.
E-mail address: mike@nsstc.uah.edu (M.J. Newchurch).

0022-4073/$ - see front matter © 2003 Elsevier Ltd. All rights reserved.
doi:10.1016/S0022-4073(03)00231-0

Nomenclature

AICO	Actual Intra-Cloud Ozone
AZA	Relative Azimuthal Zenith Angle
BCOA	Below Cloud Ozone Absorption
CBH	Cloud-Base Height
CGD	Cloud Geometrical Depth
COD	Cloud Optical Depth
COP	Cloud Optical Property
CTH	Cloud-Top Height
CTP	Cloud-Top Pressure
DU	Dobson Unit
ECF	Effective Cloud Fraction
EICO	Effective Intra-Cloud Ozone
FCF	Forward Cloud Fraction
GOME	Global Ozone Monitoring Experiment
HEX	HEXagon column ice crystals
ICOAEN	Intra-Cloud Ozone Absorption ENhancement
ISCCP	International Satellite Cloud Climatology Project
OMI	Ozone Monitoring Instrument
ORE	Ozone Retrieval Error
OZAC	OZone Above Clouds
OZBC	OZone Below Clouds
PCM	Partial Cloud Model
POLY	POLYcrystals
PPGSRAD	Polarized Plane-parallel Gauss-Seidel RADiative transfer model
SCIAMACHY	SCanning Imaging Absorption SpectroMeter for Atmospheric ChartographY
SHADOZ	Southern Hemisphere ADditional OZonesondes
SZA	Solar Zenith Angle
TOC	Total Ozone Column
TOMRAD	TOMS RADiative transfer model
TOMS	Total Ozone Mapping Spectrometer
V7	Version-7
VZA	View Zenith Angle
WC	Water Clouds
WCHG	Water Clouds with Henyey–Greenstein phase function

1. Introduction

More than half of Earth's surface is usually covered with clouds [1]. Accurate retrieval of atmospheric constituents over cloudy areas is very important in determining the overall retrieval accuracy from satellite, aircraft, or ground remote sensing measurements. However, accurate retrieval over

cloudy areas is very complicated in the ultraviolet, visible, and infrared spectral region and remains a most challenging goal. First, clouds prevent instruments from accurately measuring constituents above clouds (e.g., for ground measurements) or below clouds (e.g., for space-borne measurements). Second, microphysical (e.g., effective particle radius, shape, composition, and phase) and macrophysical (e.g., cloud-top height, cloud fractional coverage, cloud optical depth, and cloud morphology) characteristics of clouds, which are required for accurately evaluating the observed radiances from such instruments, are not easily available and are highly variable both temporally and spatially. Therefore, most retrieval algorithms of trace gases highly idealize clouds [2,3]. However, detailed studies are required to examine the effects of these idealizations on retrieval accuracy.

The Total Ozone Mapping Spectrometer (TOMS) Version-7 (V7) algorithm assumes optically thick clouds (cloud reflectivity $\geqslant$ 80%) as opaque Lambertian surfaces, employs a Partial Cloud Model (PCM), and determines the Cloud-Top Pressures (CTPs) from monthly mean International Satellite Cloud Climatology Project (ISCCP) cloud data. Newchurch et al. [4] studied ozone retrieval errors (OREs) caused by incorrect CTPs, and found unexplained above-cloud ozone excess of 4–9 Dobson Units (DU) (1 DU $= 2.69 \times 10^{16}$ molecules cm^{-2}) compared to ozone in neighboring clear areas. They speculated that the assumption of opaque Lambertian clouds causes the unexplained cloudy ozone excess. Actual clouds are not Lambertian even for optically thick clouds [5,6]. The assumption of angularly independent cloud surfaces might lead to OREs. Also, photons can penetrate the clouds, and the coupling of multiple scattering and absorption in the clouds results in a strong absorption enhancement [7,8]. As for ground-based zenith-sky or global irradiance measurements, the absorption path length can be enhanced by a factor of up to 10 [6,8,9]. Consistently, abnormal increases up to 200 DU in the derived ozone have been reported in many studies over heavily cloudy skies without taking in-cloud multiple scattering effects into account [8,10–12]. As for space-borne measured backscattered radiation, the path enhancement is relatively smaller, typically about a factor of 2 [6]. The absorption enhancement in the clouds was also recognized as a limiting factor in accurately retrieving CTPs from the backscattered radiances in and around O_2-A band [13–15]. Neglecting photon penetration inside clouds can lead to a significant error in the retrieved CTP by up to 200 hPa [14,15]. As for ozone retrieval from backscattered radiances, significant errors can occur if the amount of ozone in the clouds is significant. In the TOMS V7 PCM, a pixel with reflectivity from 8% to 80% is treated as a linear combination of a cloudy scene of cloud reflectivity 80% and a clear scene of ground reflectivity 8% with the Effective Cloud Fraction (ECF) as a free parameter [16]. The 8% and 80% values are selected during the TOMS V7 algorithm development by minimizing known errors in the retrieval. This PCM will be applied in the future Ozone Monitoring Instrument (OMI) products for retrieving ozone and other trace gases [2,3]. In reality, the reflectivity of the cloud part might be much smaller than 80% but with a larger cloud fraction, or it might have a larger cloud reflectivity but with a smaller cloud fraction. The uncertainty in cloud fraction and cloud reflectivity might cause significant OREs. Therefore, the assumption of 80% as minimum full-cloud reflectivity needs to be evaluated in terms of ozone retrieval.

Koelemeijer and Stammes [17] investigated the effects of clouds on ozone retrieval from Global Ozone Monitoring Experiment (GOME) measurements. They found that the influence of clouds on the retrieved Total Ozone Column (TOC) depends primarily on the Cloud-Top Height (CTH), Cloud Optical Depth (COD), and cloud fraction. Some of the effects of clouds on GOME measurements are expected on TOMS measurements as well. But some effects of clouds might be different on TOMS measurements because the GOME instrument and the ozone retrieval method are very different. One

limitation in these authors' analysis of cloud effects is that they assume the Cloud Geometrical Depth (CGD) to be 1 km. Because the amount of ozone in a 1-km cloud is small, the assumption of 1-km clouds can largely underestimate the large enhanced ozone absorption inside geometrically thick clouds.

This paper investigates the effects of assuming opaque Lambertian clouds and employing the PCM on ozone retrieval, with a particular focus on errors over tropical high-reflectivity convective clouds. In Section 2, we describe the radiative transfer models and model setups. Section 3 gives the methodology. We present the results in Section 4 and summarize this study in Section 5.

2. Radiative transfer models and model setups

We use the Polarized Plane-parallel Gauss-Seidel RADiative transfer model (PPGSRAD) [18], which treats clouds as scattering media, to simulate measured backscattered radiances, and use the TOMS V7 algorithm to retrieve TOC. The forward model TOMS RADiative transfer model (TOMRAD) calculates the look-up table radiances for the TOMS V7 algorithm. One major difference about cloud treatment is that TOMRAD treats clouds as Lambertian surfaces but PPGSRAD can treat clouds as scattering media by specifying single scattering albedo, asymmetry factor, phase matrix, CTH, and Cloud-Base Height (CBH).

To reduce the model bias between PPGSRAD and TOMRAD, all the input parameters to these models are the same as much as possible except for clouds. The ozone absorption coefficients [19,20], Rayleigh scattering coefficients [21], and molecular depolarization factors [21] used in the TOMS V7 algorithm are used in PPGSRAD. Look-up table radiances in the operational TOMS V7 algorithm are the sum of radiances at forty-five 0.05-nm intervals across each of the 1.1-nm TOMS bandwidths weighted by solar flux and a triangular slit function. However, it is impractical to do such calculation in PPGSRAD for cloudy-sky conditions because of the computation burden. Instead, effective coefficients are derived by weighting the corresponding spectral coefficients across each 1.1-nm bandwidth of NIMBUS-7 and Earth-Probe TOMS by the product of solar flux and a triangular slit function. Correspondingly, these effective coefficients are also used to recalculate the look-up table radiances in the TOMS V7 algorithm. The original look-up table contains radiances calculated only at 1.0 and 0.4 atm. To avoid the radiation interpolation error identified by Newchurch et al. [4], the look-up table radiances are calculated at 10 pressure levels from 1 to 0.1 atm at 0.1-atm intervals. The use of 10 pressure levels reduces radiance interpolation errors to within 0.1 DU under most conditions. The interpolated TOMS standard climatological ozone and temperature profiles [16] are used consistently in both TOMRAD and PPGSRAD. Polarization is always considered in TOMRAD. In PPGSRAD, we usually include polarization unless the neglect of polarization will not affect results.

Clouds are treated as homogeneous and plane-parallel, and the cloud phase can be liquid, ice, or mix-phased. In PPGSRAD, we treat clouds as either Water Clouds (WC) or ice clouds. Ice clouds are modeled either as HEXagonal column ice crystals (HEX) or POLYcrystals (POLY) that represent either idealized or more realistic types of ice crystals. POLY, a randomized version of the second-generation triadic Koch fractal, proposed by Macke et al. [22], is adopted in the ISCCP retrieval algorithm for ice clouds. The refractive indices are obtained from Hale and Querry [23] for WC. Han et al. [24] made a global survey of WC and found the average effective radius is

Table 1
Refractive indexes and optical properties for water clouds

Wavelength (μm)	Refractive index		Asymmetry factor (g)	Single scattering albedo (ω_0)
	Real	Imaginary		
0.3086	1.3479	1.405E − 8	0.8674	0.9999947
0.3123	1.3474	1.327E − 8	0.8675	0.9999950
0.3174	1.3469	1.227E − 8	0.8674	0.9999955
0.3224	1.3463	1.130E − 8	0.8673	0.9999959
0.3311	1.3453	9.678E − 9	0.8674	0.9999965
0.3397	1.3442	8.158E − 9	0.8674	0.9999971
0.3599	1.3421	5.148E − 9	0.8675	0.9999983
0.3800	1.3406	3.072E − 9	0.8672	0.9999988

Table 2
Refractive indexes and optical properties for HEX and POLY

Wavelength (μm)	Refractive index		Hexagonal column ice crystals (HEX)		Polycrystals (POLY)	
	Real	Imaginary	ω_0	g	ω_0	g
0.3123	1.3314	5.012E − 9	0.9999927	0.7972	0.9999962	0.7320
0.3174	1.3304	4.825E − 9	0.9999930	0.7985	0.9999964	0.7305
0.3311	1.3279	4.345E − 9	0.9999940	0.7995	0.9999969	0.7341
0.3397	1.3265	4.069E − 9	0.9999946	0.8005	0.9999972	0.7383
0.3599	1.3235	3.503E − 9	0.9999955	0.8021	0.9999978	0.7372
0.3800	1.3212	3.053E − 9	0.9999964	0.8042	0.9999982	0.7360

$\sim$ 10 μm. Water clouds are modeled with a gamma distribution with an effective radius of 10 μm and an effective variance of 0.10 μm, a model that has been used in ISCCP cloud retrieval [25–28]. The Bohren–Huffman Mie code [29] embedded in PPGSRAD calculates optical properties (single scattering albedo, asymmetry factor, and phase matrix) for WC. Table 1 shows the refractive indices, asymmetry factor, and single scattering albedo at NIMBUS-7 and Earth-Probe TOMS wavelengths. The refractive indexes for clear ice are obtained from Warren [30]. For both HEX and POLY, a -2 power law size distribution is assumed with an effective radius of 30 μm and an effective variance of 0.1 μm [26,28,31]. The Ray Tracing code developed by Macke et al. [22] calculates optical properties for ice clouds. Table 2 shows the refractive indices and optical properties for HEX and POLY at NIMBUS-7 TOMS wavelengths. The calculated single scattering albedos, asymmetry factors, and phase matrices are comparable to those values calculated by Macke et al. [22], Mishchenko et al. [26], and Doutriaux-Boucher et al. [31].

The calculated extinction efficiency for WC is close to 2 but is slightly different at different wavelengths, so the COD for a cloud varies slightly with wavelength. For example, a cloud with a COD of 40 at 312.34 nm has a COD of 40.17 at 380 nm. The extinction efficiency for ice clouds is assumed to be 2, so the COD is wavelength invariant. The COD values in the following context refer to values at 312.34 nm.

Radiances are calculated at Solar Zenith Angle (SZA) $\theta_0 = 0°$, 15°, 30°, 45°, 60°, 70°, and 75°; View Zenith Angle (VZA) θ from 0° to 70° every 5°; and relative Azimuthal Zenith Angle (AZA) $\Phi = 0°$, 30°, 60°, 90°, 120°, 150°, and 180°. The average values and standard deviation values seen in the following context are the statistics from all the above viewing geometry.

Although the input parameters are consistent in both TOMRAD and PPGSRAD as much as possible, there is bias between these two models. Under clear-sky conditions, when we can compare radiances calculated by both models, the radiances from PPGSRAD are smaller by $0.21 \pm 0.06\%$ (the value following "±" is the 1 standard deviation value) and $0.16 \pm 0.08\%$ at 312.34 nm on average over all the viewing geometry for surface reflectivity 8% and 80%, respectively. Correspondingly, errors in retrieved ozone are 0.65 ± 0.20 and 0.35 ± 0.20 DU, respectively. These errors in both radiances and retrieved ozone are relatively small compared to errors of our concern. In addition, we have seen violation of conservation of energy (i.e., photon losses) at the surface for thick clouds when using PPGSRAD in a conservative scattering case, but we observe conservation of energy to within 1.0E−5 for irradiances at top of the atmosphere. And past comparisons have shown agreement with radiances calculated using discrete ordinate transfer models at the top of the atmosphere, even with this "disappearing photons" problem.

3. Methodology

To have a clear understanding of how assuming opaque Lambertian clouds causes OREs, we divide the effects into four categories. The effect of assuming angularly independent cloud reflection on ozone retrieval is called the "Lambertian effect". OREs resulting from the retrieved incorrect cloud fraction when using the PCM are called the "PCM effect". We call the sum of Lambertian and PCM effects the "Lambertian-PCM effect". OREs caused by actual ozone absorption enhancement in clouds are called the "Intra-Cloud Ozone Absorption ENhancement (ICOAEN) effect", which can be considered as the Effective Intra-Cloud Ozone (EICO) seen from the instrument. Similarly, OREs due to actual ozone absorption below cloud bottoms by backscattered photons is called the "Below-Cloud Ozone Absorption (BCOA) effect". The sum of ICOAEN and BCOA effects is called the "opaque effect".

Fig. 1 compares the actual scene setup in the forward simulation and the corresponding scene assumed in the TOMS V7 algorithm. In the forward calculation, the cloud fraction is set as 1 with CTP P_c. However, in the TOMS V7 retrieval, the scene is assumed to be a cloudy sky of reflectivity $\geqslant 80\%$ at P_c with a cloud fraction f_c ($0 \leqslant f_c \leqslant 1$) and a clear sky of surface reflectivity $\leqslant 8\%$ with a fraction $1 - f_c$. If $0 < f_c < 1$, the cloud reflectivity is 80% and the ground reflectivity is 8%. In Fig. 1, Ω_t, Ω_a, and Ω_b are the TOC, Ozone Above Clouds (OZAC), and Ozone Below Clouds (OZBC), respectively, from the given ozone profile. In the retrieval, the retrieved TOC Ω'_t still consists of two parts: the added OZBC (Ω'_b) and the directly retrieved ozone (Ω'_a). The Ω'_b, which is reported in the TOMS V7 level-2 data, is approximately the product of Ω_b and f_c as long as the ozone profile for ozone retrieval is not very different from the ozone profile used in forward simulation. If the actual cloud is opaque and the ozone retrieval is perfect, Ω'_a should be equal to Ω_a with Ω'_b equal to Ω_b. Corresponding to the fact that the retrieved ozone consists of two parts, the error in TOC ($\Delta\Omega_t$) is decomposed into the error in OZAC ($\Delta\Omega_a$) and the error in OZBC ($\Delta\Omega_b$). These errors $\Delta\Omega_t$, $\Delta\Omega_a$, and $\Delta\Omega_b$ are defined as the difference between the retrieved quantities and

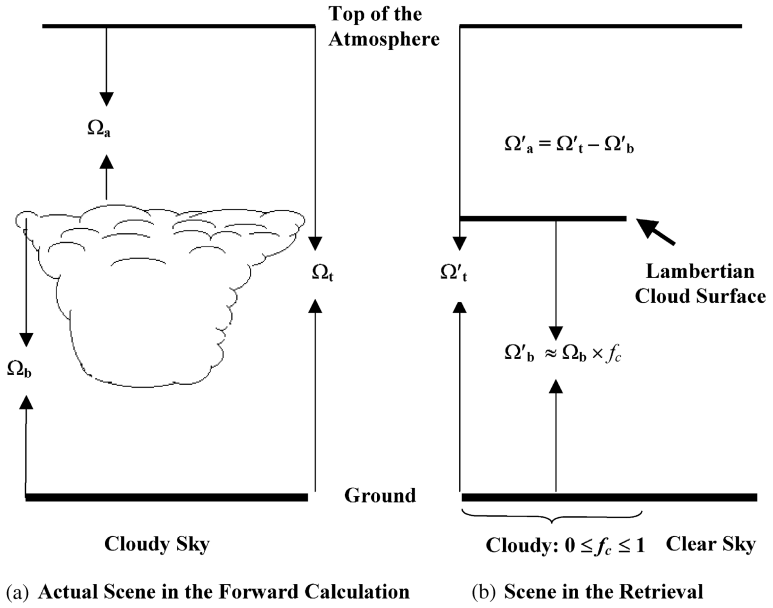

Fig. 1. Comparison of scenes between forward simulation and retrieval. (a) Full cloudy scene in the forward calculation. (b) Assumed scene in the TOMS retrieval.

the forward-calculation quantities as follows:

$$\Delta\Omega_x = \Omega'_x - \Omega_x, \quad x = t, a, b. \tag{1}$$

If no ozone is placed below the cloud top, the ICOAEN and BCOA effects are zero. This configuration simulates an opaque cloud in terms of ozone absorption although photons still penetrate the cloud. Therefore, we can study the effect due to Lambertian and PCM effects. The forward radiances calculated using PPGSRAD are inverted to retrieve the TOC. The difference between the retrieved and input TOC gives the Lambertian-PCM effect. Although the ozone below clouds is treated as nonexistent to simulate opaque clouds, it is included in the input TOC. If the ECF is forced to be the a priori cloud fraction by modification of the TOMS V7 algorithm, the PCM effect diminishes to zero and only the Lambertian effect exists. Assuming that the PCM and Lambertian effects are independent, we can obtain the PCM effect by subtracting the Lambertian effect from the Lambertian-PCM effect. To investigate the ICOAEN effect only, two sets of backscattered radiances are calculated using PPGSRAD, with and without intra-cloud ozone, respectively. The difference between the retrieved TOC with and without ozone gives the ICOAEN effect. This method of comparing the cases with and without absorbers (or absorption) in the cloud has been applied to study absorption and effective path length enhancements in clouds [6,8,14,32]. Similarly, the BCOA effect can be obtained by comparing the difference in the retrieved ozone between simulations with and without ozone below the cloud base in the forward simulation.

We determine the base case for radiance simulation from tropical deep convective clouds. Analysis of ISCCP D1 cloud data for deep convective clouds in the tropics (10°S–10°N) in October 1983 indicates that COD values for these clouds range from 23 to 379 with a mean value of 44.2 ± 18.4

and CTPs range from 127 hPa to 503 hPa with a mean value of 252.8 ± 84.9 hPa [28]. The average cloud-top albedo (the ratio of upward flux to downward flux) for a WC of COD 40 ranges from 77% to 88% when the SZA increases from 0° to 75°. The average albedos are close to 80%, indicating that the TOMS V7 algorithm treats such a scene as nearly overcast or overcast. Based on ISCCP observations and the TOMS PCM, we choose a WC with a COD of 40 positioned at 2–12 km to represent a typical cloud for this study. We typically treat clouds as WC because there is a large uncertainty in the optical properties of ice clouds and because water clouds are most commonly used in applications. The TOMS standard low-latitude ozone profile L275 (i.e., with a TOC of 275 DU) is used as a representative profile. Ground surface pressure is fixed at 1.0 atm. Typically, radiance calculation is done at NIMBUS-7 TOMS wavelengths (312.3, 317.4, 331.1, 339.7, 359.9, and 380.0 nm). We test the sensitivities of OREs to Cloud Optical Properties (COPs), COD, cloud locations, ozone amount and distribution in the clouds, atmospheric profiles, and measurement wavelengths (e.g., NIMBUS-7 vs. Earth-Probe TOMS. Earth-Probe TOMS measures radiances at 308.6, 312.6, 317.6, 322.4, 331.3 and 360.4 nm). Sections 4.1–4.4 present results for forward full clouds (i.e., cloud fraction is assumed to be 1 in the forward simulation) and Section 4.5 discusses how OREs vary with Forward Cloud Fractions (FCFs, i.e., cloud fractions assumed in forward simulations).

4. Results and discussion

4.1. Lambertian and PCM effects

Fig. 2 shows the distributions of $\Delta\Omega_t$ for the base condition. The TOMS standard ozone profile L275 is used except that OZBC is forced to be zero to exclude ozone absorption below clouds. The error distributions represent the Lambertian-PCM effects. The error patterns are dependent on SZA, VZA, and AZA. The $\Delta\Omega_t$ ranges from -4.1 to 4.4 DU with an average error of -0.8 ± 1.1 DU. Fig. 3a shows the $\Delta\Omega_t$, $\Delta\Omega_a$, and $\Delta\Omega_b$ due to Lambertian-PCM effect as a function of ECF. We can see that $\Delta\Omega_a$ is mainly positive and $\Delta\Omega_b$ is mainly negative except at the ECF of 1. These two errors usually cancel each other, leading to smaller errors in the TOC. With decreasing ECF, both $\Delta\Omega_a$ and $\Delta\Omega_b$ increase in their magnitudes. At the EFC of 1, $\Delta\Omega_b$ varies from -2 to 7 DU mainly because of profile difference between retrieval and forward calculation. At large geometrical path length (i.e., $\sec\theta_0 + \sec\theta$), higher-latitude profiles with more tropospheric ozone could be used in the retrieval, thus leading to large positive errors up to ~ 7 DU.

Fig. 3b shows the $\Delta\Omega_t$, $\Delta\Omega_a$, and $\Delta\Omega_b$ due to the Lambertian effect as a function of geometrical path length when the ECF is forced to be 1. $\Delta\Omega_t$ is very close to $\Delta\Omega_a$ except at larger viewing geometry where $\Delta\Omega_b$ is not zero. The Lambertian effect ranges from -4.1 to 4.4 DU with an average error of 0.2 ± 1.3 DU.

The difference between Figs. 3a and b indicates the PCM effect, shown in Fig. 3c. Errors are zero at the ECF of 1 just because of the definition of the PCM effect. The positive $\Delta\Omega_a$ and negative $\Delta\Omega_b$ effects almost cancel, leading to a much smaller PCM effect. It is straightforward that $\Delta\Omega_b$ increases in magnitude with decreasing ECF according to its definition.

Table 3 shows error ranges and average errors arising from the Lambertian and PCM effects for different COPs, CODs, cloud locations, atmospheric ozone profiles, and measurement wavelengths.

Table 3
Average values and ranges of Lambertian-PCM, Lambertian, and PCM effects

					Lambertian-PCM effects		Lambertian effect		PCM effect	
	Cloud type	Profile	Cloud COD	Location (km)	Error range (DU)	Avg. error ± 1 s.d. (DU)	Error range (DU)	Avg. error ± 1s.d. (DU)	Error range (DU)	Avg. error ± 1 s.d. (DU)
Base case	WC	L275	40	2–12	−4.1–4.4	−0.8 ± 1.1	−4.1–4.4	−0.2 ± 1.3	−3.0–0.4	−0.5 ± 0.8
Optical properties	WCHG	L275	40	2–12	−9.8–4.8	−0.6 ± 1.0	−4.6–4.8	0.1 ± 1.2	−8.2–0.0	−0.7 ± 1.2
	HEX	L275	40	2–12	−7.6–10.9	−0.1 ± 1.3	−7.6–10.9	0.0 ± 1.4	−1.6–0.3	−0.2 ± 0.3
	POLY	L275	40	2–12	−2.8–3.3	1.4 ± 1.2	−2.8–3.3	1.4 ± 1.2	−0.8–0.4	0.0 ± 0.1
COD	WC	L275	1	2–12	−18.3–4.0	−12.4 ± 3.6	−3.4–10.0	6.0 ± 2.5	−22.3–0.0	−18.4 ± 4.1
	WC	L275	2	2–12	−16.8–2.7	−11.0 ± 3.3	−4.3–8.5	4.2 ± 2.4	−18.9–0.0	−15.2 ± 3.9
	WC	L275	5	2–12	−12.5–4.9	−8.1 ± 2.7	−3.9–6.1	1.3 ± 2.0	−13.9–0.3	−9.4 ± 2.8
	WC	L275	10	2–12	−8.0–4.9	−5.2 ± 2.1	−4.1–4.8	0.0 ± 1.8	−9.5–0.0	−5.2 ± 2.0
	WC	L275	20	2–12	−4.6–4.7	−2.4 ± 1.5	−4.4–4.7	−0.3 ± 1.5	−5.6–0.0	−2.2 ± 1.3
	WC	L275	100	2–12	−4.0–4.0	−0.3 ± 1.2	−4.0–4.0	−0.2 ± 1.2	−1.2–0.0	−0.1 ± 0.3
Cloud location	WC	L275	40	2–3	−12.2–4.2	1.1 ± 2.0	−12.2–4.5	1.3 ± 2.1	−0.8–0.0	−0.2 ± 0.2
	WC	L275	40	2–7	−7.2–3.9	0.4 ± 1.3	−7.2–4.2	0.7 ± 1.6	−1.3–0.0	−0.3 ± 0.4
	WC	L275	40	11–12	−4.1–3.9	−0.8 ± 1.2	−4.1–3.9	−0.2 ± 1.4	−3.0–0.3	−0.6 ± 0.8
	WC	L275	40	7–12	−4.1–3.9	−0.8 ± 1.2	−4.2–4.4	−0.2 ± 1.4	−3.0–0.4	−0.6 ± 0.8
Profile	WC	L225	40	2–12	−3.0–2.4	−0.9 ± 0.9	−3.1–2.5	−0.4 ± 1.1	−2.6–0.0	−0.5 ± 0.7
	WC	L325	40	2–12	−5.7–6.7	−0.7 ± 1.4	−5.7–6.7	−0.2 ± 1.6	−2.9–0.0	−0.5 ± 0.7
	WC	M325	40	2–12	−10.1–4.4	−1.7 ± 2.8	−10.4–4.2	−1.8 ± 2.7	−10.6–3.0	0.10 ± 3.6
	WC	M375	40	2–12	−11.2–4.8	−1.8 ± 3.3	−11.5–7.1	−2.0 ± 3.2	−11.4–4.4	0.2 ± 4.5
	WC	M425	40	2–12	−11.7–8.0	−3.7 ± 3.4	−11.7–11.0	−2.3 ± 4.2	−8.2–1.8	−1.4 ± 2.0
Earth-probe	WC	L275	40	2–12	−10.5–3.0	−0.5 ± 1.1	−4.9–3.0	−0.0 ± 1.3	−10.8–0.0	−0.5 ± 0.8

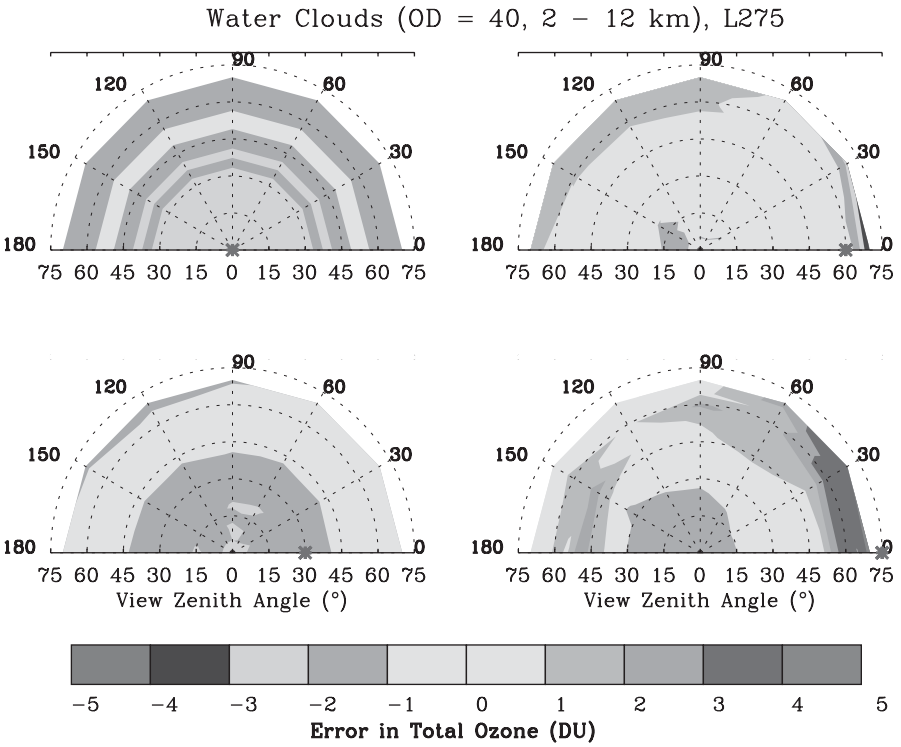

Fig. 2. Ozone retrieval errors in total ozone due to the Lambertian-PCM effect at different solar zenith angles (0°, 30°, 60°, and 75°) for a water cloud of optical depth 40 at 2–12 km. The low-latitude ozone file L275 is used except that no ozone is put below the cloud top. The asterisk symbol on the *x*-axis indicates the solar zenith angle.

It should be noted that some cloud setups are unreasonable and are shown for illustration only. To show how the Lambertian and PCM effects vary with COPs, we calculate results for 2–12 km clouds with COD 40 but with four different COPs: WC, Water Clouds with Henyey–Greenstein phase function (WCHG), HEX, and POLY. WC and WCHG have the same single scattering albedos and asymmetry factors but with different phase functions. The Lambertian-PCM effect shows different angular distributions for these four COPs. For HEX, there are several spots with large negative or positive errors probably arising from some spikes in the calculated phase function. However, the average errors for different COPs are within ±2 DU.

We compare the average Lambertian and PCM effects and their ranges for 2–12 km clouds with different CODs (1, 2, 5, 10, 20, 40, and 100). Because the ECF decreases with decreasing COD, the negative PCM effect increases in magnitude, from -0.2 ± 0.2 DU at COD 100 to -18.4 ± 4.1 DU at COD 1. The average Lambertian effect increases with decreasing COD, from -0.2 ± 1.2 DU at COD 100 to 6.0 ± 2.5 DU at COD 1. At smaller CODs, the Lambertian-PCM effect is dominated by the negative PCM effect.

Four cloud locations (2–3, 2–7, 11–12, and 7–12 km) along with the base condition are used to show how the Lambertian and PCM effects vary with cloud locations. Model setups other than cloud

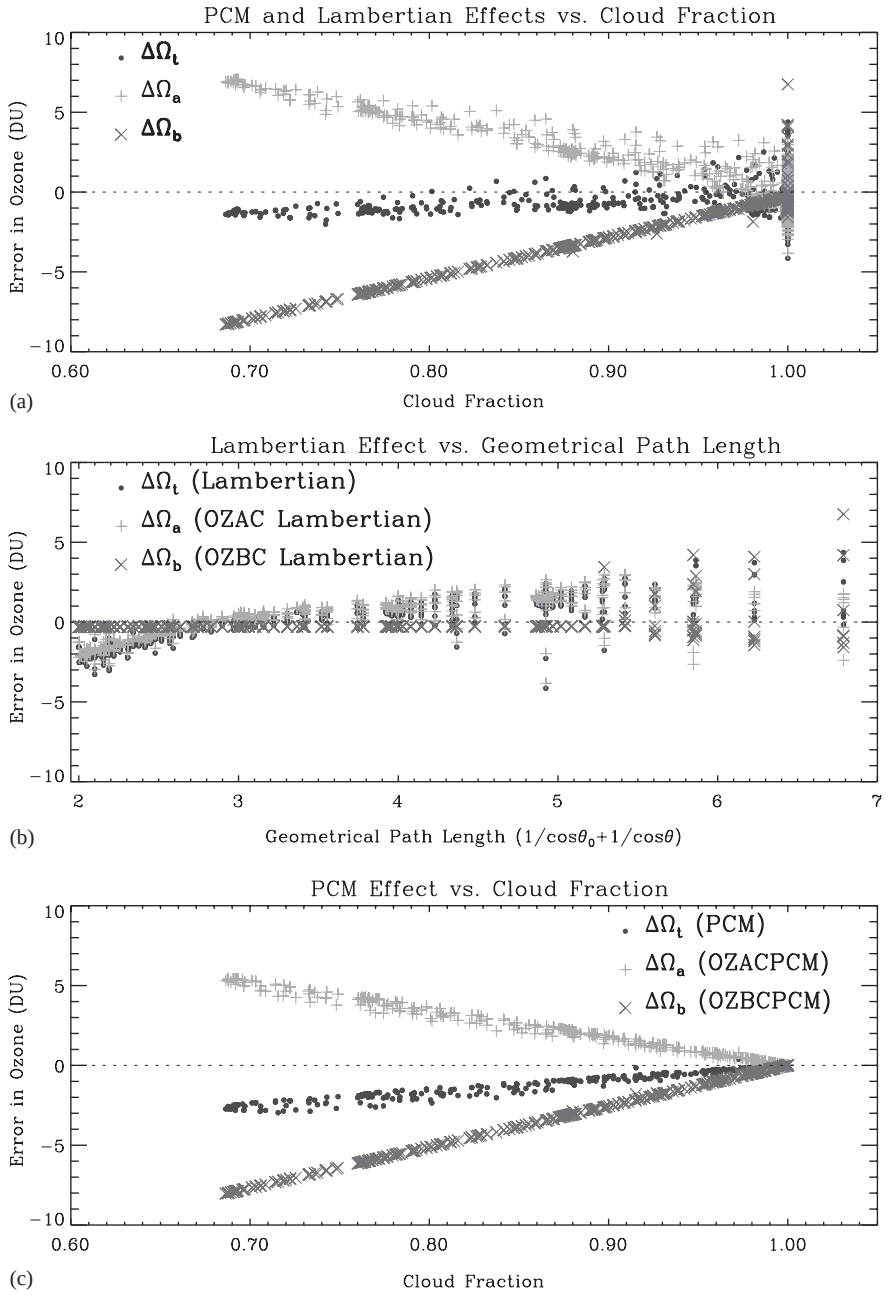

Fig. 3. Lambertian and PCM effects for a 2–12 km water cloud of optical depth 40. (a) The Lambertian-PCM effect as a function of derived effective cloud fraction. (b) The Lambertian effect as a function of geometrical path length. (c) The PCM effect as a function of derived effective cloud fraction.

location are the same. The Lambertian and PCM effects do not change with CBH if the CTH is the same. With decreasing CTH, the Lambertian effect becomes more scattered. The errors are more positive at most angles, but are more negative at several large SZAs and VZAs on the solar side. However, the average errors for these clouds are all within ± 2 DU.

We test the sensitivity of the Lambertian and PCM effects to varying ozone profiles (L225, L325, M325, M375, and M425). "L" and "M" stand for low-latitude and mid-latitude, respectively. The three digits represent the TOC of the ozone profile. The latitudes assumed in ozone retrieval are 0° and 45° for using low- and mid-latitude profiles, respectively. With increasing TOC in ozone profiles, both the Lambertian and PCM effects are slightly more scattered. Especially, errors using mid-latitude ozone profiles are much more scattered and less orderly compared to errors using low-latitude ozone profiles because of the used profile-mixing scheme in the TOMS V7 algorithm. However, the average errors are within 1.5% of the TOC for these ozone profiles. We investigate the Lambertian and PCM effects at Earth-Probe TOMS wavelengths and find almost no difference from NIMBUS-7 wavelengths.

According to the above results, the Lambertian and PCM effects vary with viewing geometry, COP, COD, CTH, and ozone profile. Although the triplet method in the TOMS V7 algorithm, which retrieves ozone from measured radiances at ozone-sensitive, ozone weak absorbing, and ozone non-absorbing wavelengths can greatly reduce errors caused by assuming Lambertian clouds, several factors can cause the observed OREs. Forward calculation assumes scattering clouds while retrieval assumes Lambertian clouds; ozone profiles could be different between forward calculation and retrieval; the ECF is different from the actual cloud fraction. The air mass factors could therefore be different between forward and retrieval scenes and therefore errors occur in the directly retrieved part of the ozone (i.e., OZAC). The slightly nonlinear wavelength-dependence in the cloud reflection might also cause some OREs in OZAC. The profile and cloud fraction difference between retrieval and simulation can cause large errors in the added OZBC. However, OREs due to the Lambertian-PCM effect are usually within 1.5% of the TOC, i.e., within the TOMS retrieval precision [16], under different conditions except when COD < 20.

4.2. ICOAEN effect

Fig. 4 shows the ICOAEN effect as a function of viewing geometry for the base condition. The a priori amount of ozone in the 2–12 km cloud from TOMS standard ozone profile L275 is 20.8 DU, but we homogeneously redistribute the intra-cloud ozone amount. The EICO ranges from 0 to 18.6 DU. The ICOAEN effect is essentially azimuthally independent but strongly dependent on the SZA and VZA, consistent with the results by Saiedy et al. [14]. The exchange of SZA and VZA does not change the EICO. The larger the SZA and VZA, usually the smaller the EICO will be. For example, the EICO is 17.7 DU at $\theta_0 = 0^\circ$ and $\theta = 0^\circ$ and is ~ 2.6 DU at $\theta_0 = 75^\circ$ and $\theta = 60^\circ$. The largest EICO of 18.6 DU occurs not exactly at nadir view but at $\theta_0 = 0^\circ$ and $\theta = 5^\circ$. Because of the backscattering peak at the scattering angle of 180° in the phase function for WC, photons penetrate less at nadir and the EICO is smaller at the nadir view than at $\theta_0 = 0^\circ$ and $\theta = 5^\circ$. The fact that the highest EICO of 18.6 DU is close to the a priori ozone in the cloud indicates that the sensor can effectively see almost all the intra-cloud ozone under these conditions.

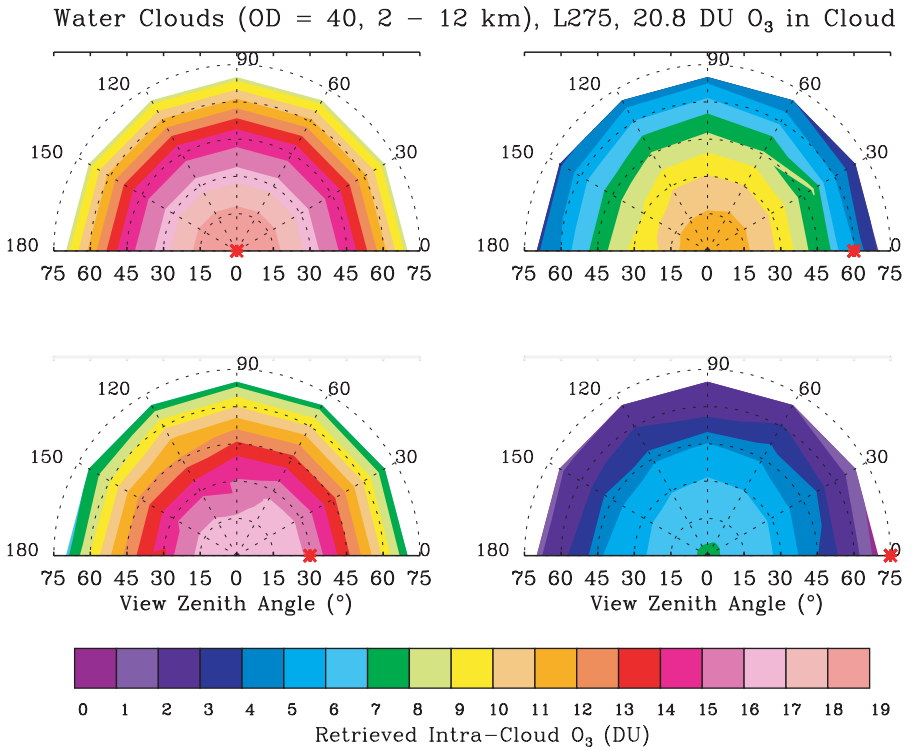

Fig. 4. Retrieved effective intra-cloud ozone as a function of viewing geometry for a 2–12 km water cloud of cloud optical depth 40. The low-latitude ozone profile L275 is used except that the 20.8 DU intra-cloud ozone is homogeneously distributed. The red asterisk symbol on the x-axis indicates the solar zenith angle.

The ratio of the two sets of calculated radiances at ozone-absorbing wavelengths indicates ozone absorption optical thickness τ_{O_3} inside the clouds [6,8]:

$$\frac{I_{O_3}}{I_{\text{no}\,O_3}} \approx \exp(-\tau_{O_3}), \tag{2}$$

where I_{O_3} and $I_{\text{no}\,O_3}$ are the calculated backscattered radiance at the top of the atmosphere for radiances with and without ozone in clouds, respectively. The above equation assumes that the absorption inside clouds is sufficiently smaller so that scattering and absorption can be considered as independent processes [6]. In our case, the average ozone absorption coefficient at 317 nm for 20.8 DU homogeneously inside clouds is fairly small, only 1.89×10^{-3} km^{-1}. Therefore, we can apply Eq. (2) to directly derive the ICOAEN effect. If we know the ozone absorption optical thickness per DU of ozone (α_{λ,O_3}), we can obtain the EICO $\Delta\Omega_{\text{calc}}$ via the following equation:

$$\frac{I_{O_3}}{I_{\text{no}\,O_3}} \approx \exp\left\{-\alpha_{\lambda,O_3}\Delta\Omega_{\text{calc}}\left(\frac{1}{\cos\theta_0}+\frac{1}{\cos\theta}\right)\right\}. \tag{3}$$

The geometrical path length is the approximate air mass factor, implicitly considered in the TOMS V7 algorithm. Eq. (3) applies even for inhomogeneous ozone distribution as long as the α_{λ,O_3} is approximately constant. Because the ozone absorption coefficient is only slightly temperature

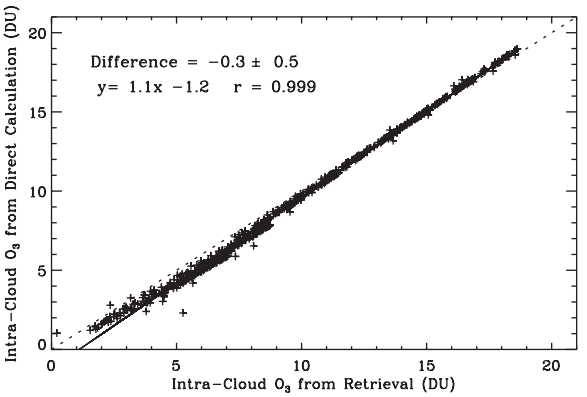

Fig. 5. Comparison of effective intra-cloud ozone between direct calculation from Eq. (3) at 317 nm and TOMS retrieval for the base condition.

dependent at 310–340 nm, we can apply Eq. (3). Fig. 5 shows a comparison of EICO between direct calculation at 317 nm using Eq. (3) and TOMS V7 retrieval (results in Fig. 4) at all the viewing geometries. There is an excellent relationship between these two calculations with a correlation of 0.999. Comparisons at other ozone-absorbing wavelengths show similar correlations as well, but the slopes and offsets are slightly different. The excellent comparison indicates that using the triplet method in the TOMS V7 algorithm cannot reduce the error induced by ozone absorption inside clouds because the photon path length in clouds does not vary much with TOMS wavelengths. Also, the good comparison suggests it is much faster to compute the ICOAEN effect from direct calculation because the radiances need to be calculated at only one ozone-absorbing wavelength.

Fig. 6a shows the ICOAEN effect as a function of VZA for WC, WCHG, HEX, and POLY, respectively, at $\theta_0 = 0°$ and 75°. The clouds and ozone profiles are the same as those in the base case except for different cloud phase functions. The ICOAEN effect does not vary much with different COPs and is within 3 DU except at nadir. The EICO at nadir is only 10.3 DU for HEX, much smaller than the EICO at $\theta_0 = 0°$ and $\theta = 15°$ (17.9 DU). This occurs because its backscattering peak is much larger than that in WC so that backscattered photons' penetration is shallower inside the clouds. Although WC and WCHG have the same asymmetry factor, the larger ICOAEN effect for WCHG arises primarily from the fact that the phase function for WCHG is smaller by a factor of five than that of WC at backscattering angle 140–180°. Among WC, HEX, and POLY, the EICO is usually largest for WC and smallest for POLY. The difference in the EICO among WC, HEX, and POLY can be explained by their difference in phase function. The larger the asymmetry factor, the smaller the backscattering, and the deeper the photons penetrate the cloud, and therefore the larger the EICO will be.

Fig. 6b shows the ICOAEN effect as a function of COD at three sets of viewing geometries. The cloud setups and ozone profiles are the same except for different CODs (0.1, 0.5, 1, 2, 5, 8, 10, 20, 30, 40, 60, 80, 100, 150, 200, 300, 400, and 500). The neglect of polarization has very little effect on the ICOAEN effect because neglecting polarization has almost the same effect on ozone retrieval for both cases with and without intra-cloud ozone. So the polarization is not included for CODs greater than 100 to reduce computation time. The EICO usually decreases with increasing

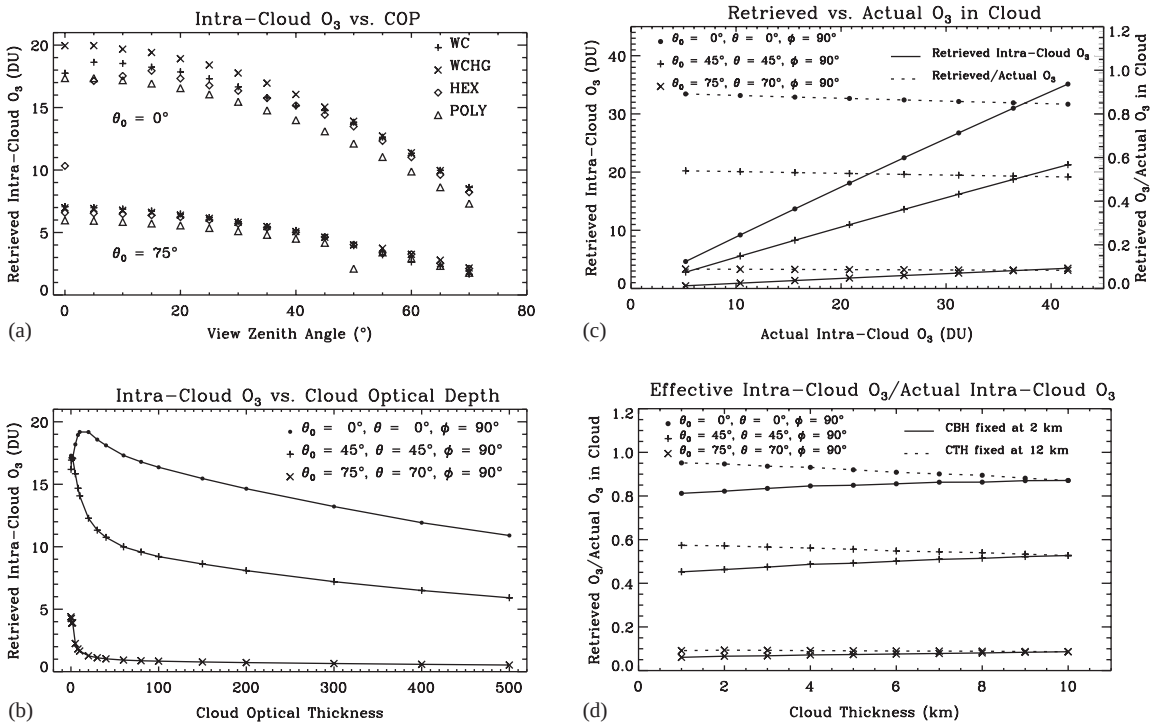

Fig. 6. Sensitivities of ICOAEN effect to various factors. (a) Effective intra-cloud ozone (EICO) vs. view zenith angle for 2–12 km clouds of optical depth 40 for water clouds, water clouds with Henyey–Greenstein phase function, hexagonal column crystals, and polycrystals at solar zenith angles 0° and 75°. (b) EICO vs. cloud optical depth for 2–12 km water clouds. (c) EICO and the ratio of EICO to Actual Intra-Cloud Ozone (AICO) vs. AICO for 2–12 km water clouds of optical thickness 40. (d) EICO and the ratio of EICO to AICO vs. cloud thickness for 2–12 km water clouds of optical thickness 40. The low-latitude ozone profile L275 is used.

COD except at small CODs. The EICO at nadir view is about 11 DU at a COD of 500, which is $\sim$ 60% of the EICO with a COD of 40 but is still significant. At nadir, the EICO peaks at COD 10 and increases with increasing COD at COD less than 10. The EICO peak shifts to a smaller COD with increasing VZAs and SZAs. The EICO peak at some intermediate CODs is related to the imperfect ozone retrieval efficiency in the lower troposphere at near-ultraviolet wavelengths when the reflectivity is small [33,34]. When the COD is very small, the cloudy atmosphere approaches a clear-sky atmosphere. The retrieved ozone for the case without ozone in the cloud is overestimated because the tropospheric part of the profile for simulation has less ozone than the TOMS standard ozone profile. The difference in the retrieved ozone between situations with and without ozone in the cloud is therefore reduced.

The solid line in Fig. 6c shows the ICOAEN effect as a function of Actual Intra-Cloud Ozone (AICO) for the base condition except with different AICO values (5.2, 10.4, 15.6, 20.8, 26.0, 31.2, 36.4, and 41.6 DU). The ICOAEN effect is strongly dependent on the AICO, and the EICO is nearly linearly proportional to the AICO. The dashed line in Fig. 6c shows that the ratio of EICO to AICO slightly decreases with increasing AICO. For example, the ratio at nadir is 0.89 and 0.84 for a priori

ozone of 5.2 and 41.6 DU, respectively. This variation with AICO is expected because the smaller the AICO, the deeper photons penetrate the cloud, and the greater is the ratio of EICO to AICO.

If the ozone profile does not change for different CGDs, the AICO increases with increasing CGD, and so does the EICO, according to Fig. 6c. Therefore, the ICOAEN effect also strongly depends on CGD. Fig. 6d shows the ratio of EICO to AICO as a function of CGD. The ozone profiles and cloud setups are the same as in the base case except that there are different CGDs and homogeneous distribution of ozone inside clouds. The ratio varies with GCD within 15%, largest for a cloud at 11–12 km (e.g., 0.95 at nadir view) and smallest for a cloud at 2–3 km (e.g., 0.81 at nadir view). The solid lines are for clouds with CBH fixed at 2 km. The larger the CGD is, the higher the CTH will be, the smaller the cloud scattering coefficient will be, and the larger the AICO will be. Wu [15] found that oxygen absorption in the cloud at 0.7609 and 0.7634 μm (i.e., oxygen-A band) increases with increasing cloud scattering coefficient for the same CODs. The increasing AICO and decreasing cloud scattering coefficient will decrease the ratio of EICO to AICO. However, the ratio in Fig. 6d increases with increasing CTH. The increase of the ratio with increasing CTH is primarily a result of interaction between cloud reflection and Rayleigh scattering above the cloud. When the CTH is lower, there is more path length enhancement above the cloud because of the stronger Rayleigh scattering. For a case without intra-cloud ozone, the radiance gain from the absence of ozone in the cloud produces more absorption above the cloud for lower-altitude clouds. The difference in the retrieved ozone between situations with and without ozone relative to AICO increases with increasing CTH. The dashed lines in Fig. 6d are for clouds with CTH fixed at 12 km. The ratio of EICO to AICO decreases with increasing CGD mainly because of the increasing AICO and decreasing cloud scattering coefficient.

We test the sensitivity of the ICOAEN effect to atmospheric ozone profiles (L225, L275, L325, M325, M375, and M425). Although the EICO values vary with different ozone profiles because the AICO changes, the ratio of EICO to AICO does not change much for different atmospheric ozone profiles. Also, the ICOAEN effect exhibits little difference between NIMBUS-7 and Earth-Probe TOMS wavelengths.

Because photons emerging at the cloud top can be backscattered from an arbitrary depth in the cloud, the ICOAEN effect should be dependent on the ozone distribution in the cloud. Fig. 7a shows five ozone profiles in a 2–12 km cloud in terms of ozone absorption coefficients at 317 nm. These ozone profiles differ from each other only in the cloud and are the same as L275 outside the clouds. These profiles are as follows: (1) original L275, (2) constant ozone mixing ratio, (3) homogeneous distribution, (4) linearly increasing ozone with altitude, (5) linearly decreasing ozone with altitude. The AICO is 20.8 DU for all the profiles. Fig. 7b shows the ICOAEN effect as a function of VZA for these ozone profiles at $\theta_0 = 30^\circ$. The ICOAEN effect is highest for the linearly increasing ozone profile and smallest for the linearly decreasing ozone profile. At $\theta = 0^\circ$, the EICO is 14.5, 13.3, 16.7, 23.1, and 10.0 DU for profiles 1–5, respectively. The EICO for the original TOMS standard profile (profile 1) is 2 DU smaller than that for the homogeneous profile (profile 3) because less ozone is distributed in the upper part of the cloud in profile 1. The EICO for the well-mixed profile (profile 2) is smaller than the EICOs for profiles 1 and 3 for similar reasons. Therefore, the ICOAEN effect is strongly dependent on ozone distribution in the clouds, and ozone distribution in the upper part of the clouds contributes more to the EICO.

Fig. 8 shows the vertical distribution of ozone absorption inside the clouds for the base condition. The cloud is divided into 20 layers, and ozone is homogeneously distributed. For each cloud layer,

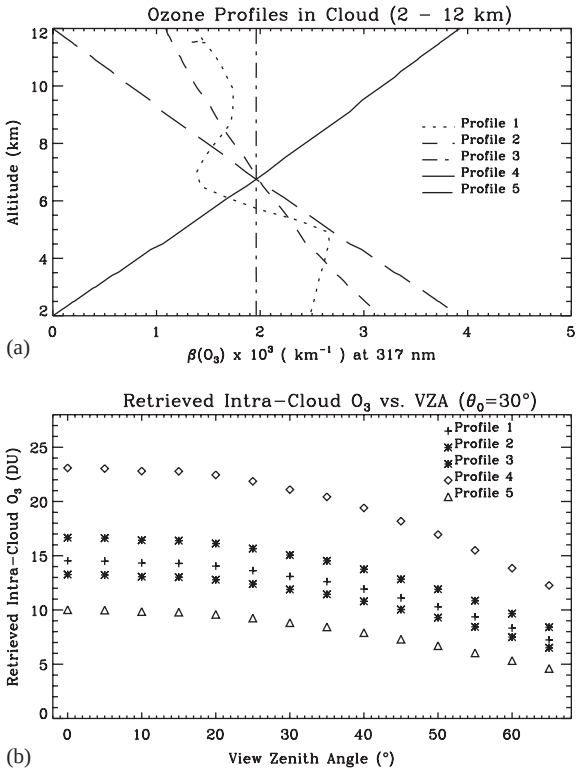

Fig. 7. (a) Ozone absorption coefficients vs. altitude for five intra-cloud ozone profiles. All profiles contain 20.8 DU ozone. (b) Retrieved intra-cloud ozone vs. view zenith angle at solar zenith angle 30° for the base case except with different intra-cloud ozone profiles as shown in (a).

two sets of radiances at 317 nm are calculated using PPGSRAD, one with ozone in the cloud except for that particular layer and the other with ozone in all layers. The difference in the retrieved ozone between these two sets of radiances indicates the EICO from the other cloud layers. The difference between the EICO for the whole cloud and the EICO from the other cloud layers approximates the contribution to ozone absorption by that particular layer. We can see that the ratios peak in the upper part of the cloud and that the peak altitude increases with increasing viewing geometries. At larger viewing geometries, the ratio peaks in the top cloud layer, indicating that the resolution of 0.5-km cloud layer is not enough to resolve the exact peak altitude. Below the peak, the ratios decrease dramatically with decreasing altitude. At smaller viewing geometries, the ratio in the upper part of the cloud can be greater than 1 because of the enhanced ozone absorption. The ratio in the lower part of the cloud is much smaller than 1 because very few backscattered photons penetrate the lower part of the cloud.

4.3. BCOA effect

The method used to obtain the BCOA effect is similar to that to obtain the ICOAEN effect except that we calculate two sets of radiances, with and without ozone below cloud bottoms. Fig. 9 shows

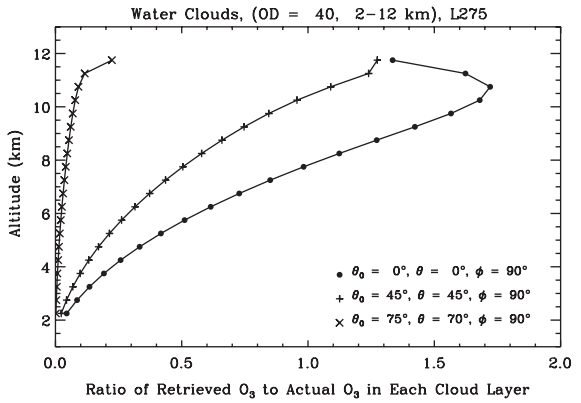

Fig. 8. Vertical distributions of ratios of retrieved effective intra-cloud ozone to actual intra-cloud ozone in each 0.5-km cloud layer for the base condition at three sets of viewing geometries.

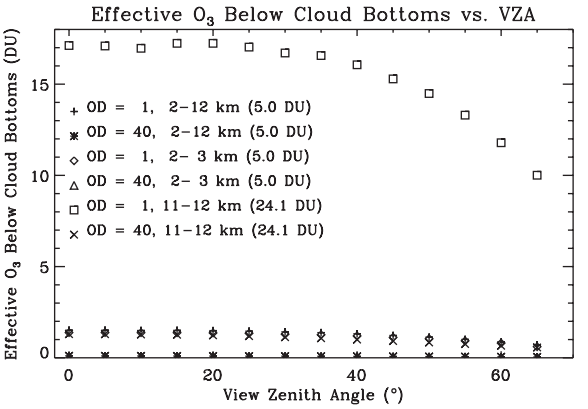

Fig. 9. Effective ozone below cloud bottoms as a function of view zenith angle for water clouds with different optical depths and cloud locations at solar zenith angle 30°. The low-latitude ozone profile L275 is used.

the BCOA effect as a function of VZA for several cloudy conditions at $\theta_0 = 30°$. Similar to the ICOAEN effect, the BCOA effect decreases with increasing SZAs and VZAs, and the SZA and VZA are interchangeable. When the BCOA effect is significant, the BCOA effect decreases strongly with increasing COD. For an 11–12 km WC at nadir view, 17.1 DU out of 24.1 DU ozone below cloud bottoms can be measured for COD 1 but only 1.3 DU for COD 40. For clouds with the same COD, the BCOA effect increases with increasing CBH, because the amount of ozone below cloud bottoms increases. The ratio of measured ozone to actual ozone below cloud bottoms decreases with decreasing CBH. For example, the ratio is about 0.71 at nadir view for a WC of COD 1 at 11–12 km but only 0.26 for a WC of COD 1 at 2–3 km. Because of more interaction among Rayleigh scattering, cloud reflection, and surface reflection below cloud bottoms with lower CBH, photons that penetrate the cloud have a smaller possibility of being backscattered to the top of the atmosphere. Overall, the BCOA becomes significant at smaller SZAs and VZAs when the cloud is optically thin and the ozone amount below the cloud bottom is large.

4.4. Overall OREs associated with clouds

Ozone retrieval errors due to the Lambertian, PCM, ICOAEN, and BCOA effects are studied in detail in Sections 4.1–4.3. This section presents the overall OREs associated with clouds, and investigates the essential effects that are primarily responsible for OREs. OREs are compared between two retrievals, one using the TOMS V7 algorithm and the other using the modified TOMS V7 algorithm by forcing the ECF to be the forward cloud fraction. The first retrieval includes all the four effects on ozone retrieval, and the second retrieval includes three effects but not the PCM effect.

Fig. 10a shows OREs from the two retrievals as a function of VZA at $\theta_0 = 30°$ for a WC of COD 1 positioned at 2–12 km. Errors in the TOC are very small using the TOMS V7 algorithm (circle) but are largely positive using the correct cloud fraction (asterisk). Using the TOMS V7 algorithm, errors in OZAC (plus) are about 20–30 DU, primarily because of the ICOAEN, Lambertian, and

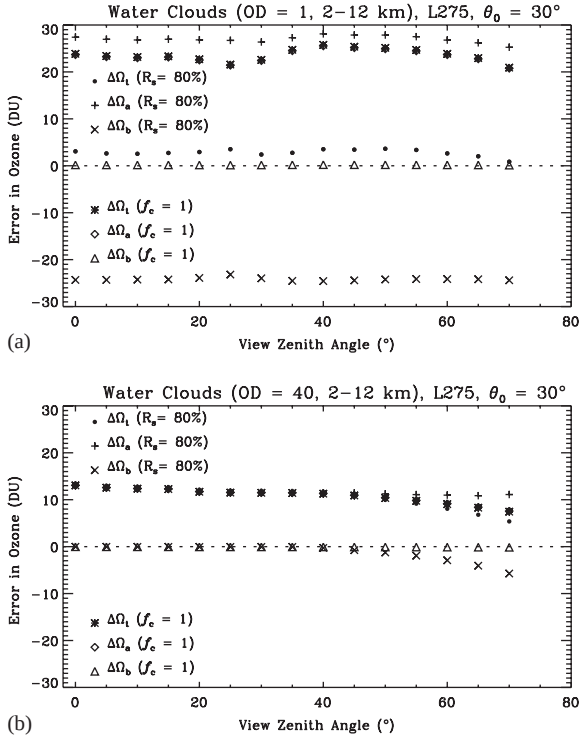

Fig. 10. Comparison of ozone retrieval errors between using the TOMS version-7 algorithm ($R_s = 80\%$) and the modified algorithm by forcing the effective cloud fraction to be the a priori cloud fraction ($f_c = 1$) at solar zenith angle 30°. (a) For the base case except at cloud optical depth 1. (b) For the base case. The $\Delta\Omega_t$, $\Delta\Omega_a$, and $\Delta\Omega_b$ indicate the error in total ozone, error in ozone above clouds, and error in ozone below clouds, respectively.

PCM effects, and errors in OZBC (cross) are about −25 DU due primarily to the PCM effect. Because of compensating errors, the TOMS V7 algorithm retrieves approximately the correct TOC. With use of the correct cloud fraction, errors in OZAC (diamond) are similar to those using the TOMS V7 algorithm, and errors in OZBC (triangle) are almost zero. The overall errors in TOC are therefore largely positive. Fig. 10b shows results similar to Fig. 10a but for COD 40. At COD 40, the derived ECF is mostly one or very close to one. Therefore, errors in ozone converge using these two retrievals. Errors in OZBC are almost zero for both retrievals. Errors in OZAC are about 10–13 DU due primarily to the ICOAEN effect. The overall errors in TOC are, therefore, largely positive due primarily to the ICOAEN effect. It should be noted that the overall OREs in TOC decrease dramatically with increasing SZAs and VZAs for optically thick clouds. For example, the ORE is about 16 DU at $\theta_0 = 0°$ and $\theta = 0°$ and about 2 DU at $\theta_0 = 75°$ and $\theta = 60°$.

Fig. 11 shows errors in TOC using the TOMS V7 algorithm for clouds at 2–12 km with different CODs at θ_0=30° and θ=30°. With increasing COD, the negative PCM effect and positive Lambertian effect decrease more dramatically in magnitude than the positive ICOAEN effect. Positive errors in TOC first increase with increasing COD until the COD reaches 20–40 when the PCM and Lambertian effects are close to zero. Then the overall error is dominated by the ICOAEN effect and slightly decreases with the further increase of COD.

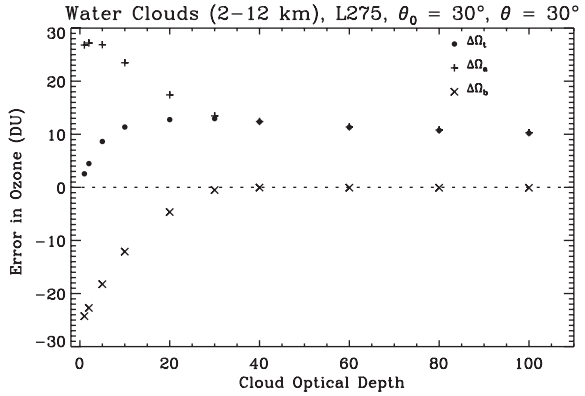

Fig. 11. Errors in total ozone (circle), ozone above clouds (plus), and ozone below clouds (cross) as a function of cloud optical depth at solar zenith angle 30° and view zenith angle 30°. The ozone profiles and cloud setups are the same as the base case except at different cloud optical depths.

Fig. 12 shows errors in TOC for COD 1 but for clouds at 2–3 and 11–12 km, respectively. In addition to the two retrievals, Fig. 12 also shows errors for retrievals assuming minimum full-cloud reflectivity as 40% and 100%, respectively. We can see that errors for more reasonable clouds at 2–3 and 11–12 km are similar to those for the cloud at 2–12 km. But the positive errors in TOC are due primarily to the Lambertian effect for the 2–3 km cloud and due primarily to the BCOA effect for the 11–12 km cloud. Assuming minimum full-cloud reflectivity to be 100% does not improve the ozone retrieval much compared to using the TOMS V7 PCM. OREs assuming reflectivity to be 40% lie between those using the TOMS V7 algorithm and the correct cloud fraction because the derived ECFs lie between those derived from the two retrievals.

According to the above results, the assumption of minimum full-cloud reflectivity to be 80% in the TOMS V7 algorithm (i.e., the TOMS V7 PCM) is fairly good because the negative PCM effect offsets other positive errors to reduce the overall errors. Especially for clouds with smaller CODs, the use of TOMS PCM leads to approximately the correct results because of compensating errors among ICOAEN, BCOA, Lambertian, and PCM effects. For optically thin clouds, the neglect of photon penetration in the clouds in the assumption of opaque clouds is largely compensated for by partial clear-sky conditions. For optically thick clouds, the PCM effect is not helpful to reduce the overall OREs, and a significant portion of the ozone below the clouds is included twice in the TOC, in both the directly retrieved OZAC and the added OZBC, leading to largely positive errors. Note that results are subject to change if the actual intra-cloud ozone amount and distribution are very different from the assumed ones (i.e., using the TOMS standard ozone profiles).

4.5. OREs associated with partial clouds

From Sections 4.1 to 4.4, the clouds in the forward simulation are assumed overcast. This section briefly discusses OREs associated with forward partial clouds. To simulate radiances for

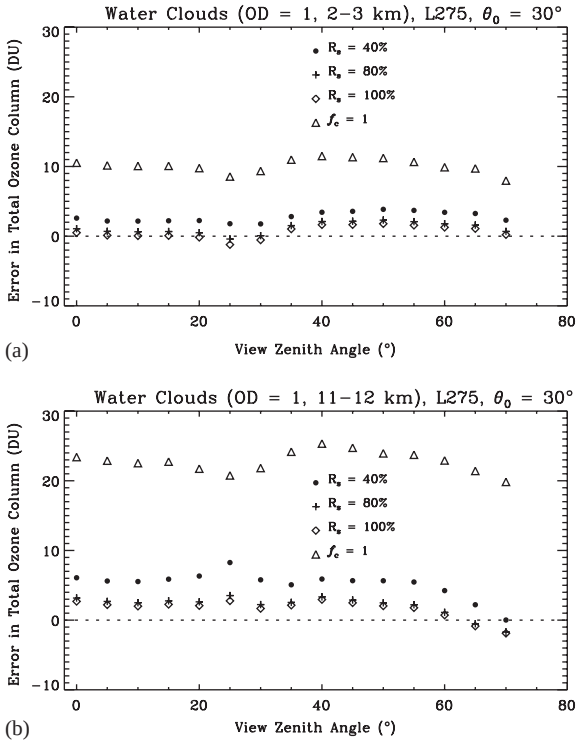

Fig. 12. Comparison of ozone retrieval errors in total ozone vs. view zenith angle among assuming minimum full-cloud reflectivity as 40%, 60%, 80% (i.e., the TOMS version-7 algorithm), 100%, and forcing the effective cloud fraction to be the a priori cloud fraction for a water cloud of cloud optical depth 1 with different cloud locations at solar zenith angle 30°. (a) A 2–3 km cloud. (b) An 11–12 km cloud. The low-latitude ozone profile L275 is used.

forward partial clouds, we employ the independent pixel approximation consistent with the TOMS V7 algorithm. The radiance for a partial cloud of cloud fraction f_c is the fraction-weighted sum of the radiances for a clear sky of ground reflectivity 8% and a cloudy sky of COD τ:

$$I(f_c, \tau, P_c) = I(\tau, P_c) \times f_c + I(R_g = 8\%, P_g) \times (1 - f_c). \quad (4)$$

The methods to obtain the Lambertian, PCM, ICOAEN, and BCOA effects for such forward partial clouds are similar to those for forward full clouds. The Lambertian effect is obtained similarly except for forcing the derived ECF to be consistent with the a priori FCF.

Fig. 13 shows the Lambertian-PCM effect (left) and the opaque effect (right) for a 2–12 km cloud of CODs 1 and 40, respectively. We can see that errors in TOC due to these different effects are proportional to FCF when errors for forward full clouds are significant. OREs are similar for other cloudy conditions. The nonlinear relationship between EICO and FCF for COD 40 is due to the large difference in the radiance between clear and cloudy conditions. Because all these effects are approximately proportional to the FCF, the overall OREs are approximately the corresponding values for full clouds but weighted by the FCF.

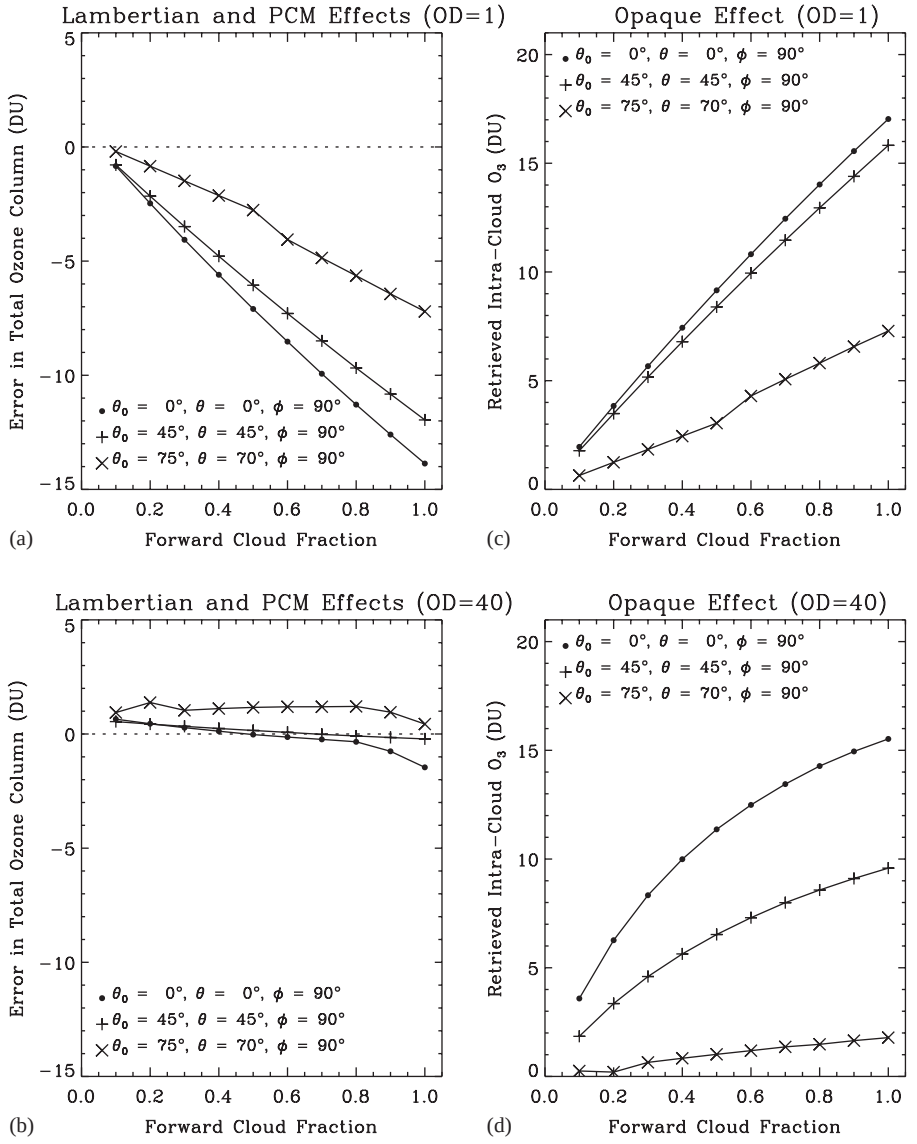

Fig. 13. Lambertian-PCM and opaque effects as a function of forward cloud fraction at three sets of viewing geometries for 2–12 km water clouds. (a) Lambertian-PCM effect for cloud optical depth 1. (b) Lambertian-PCM effect for cloud optical depth 40. (c) Opaque effect for cloud optical depth 1. (d) Opaque effect for cloud optical depth 40. The low-latitude ozone profile L275 is used.

4.6. Possibility of directly correcting OREs associated with clouds

From the above results, we know that OREs associated with clouds vary with many factors besides viewing geometry: COP, COD, CTH, CBH, ozone amount and distribution inside clouds, actual ozone

profile, and cloud fraction. Accurately correcting OREs associated with clouds in the TOMS data is impossible because most of the information is not available. Fortunately, the Lambertian, PCM, and BCOA effects are very small at COD $\geqslant 20$. At small CODs, the negative PCM effect partly offsets other positive errors, leading to approximately the correct retrieval. The cloudy conditions of most concern are probably the deep convective clouds with large COD and CGD. Correcting OREs in these scenes requires mainly knowledge of intra-cloud ozone amount and distribution, cloud optical depth, and cloud geometrical depth. With the retrieved TOMS reflectivity, we can estimate the cloud optical depth and geometrical depth by assuming some cloud types. Then the key to correcting the ICOAEN effect is the a priori knowledge of ozone amount and distribution in the clouds.

Ozone profile measurements in deep convective cloudy conditions are very limited, probably because balloons are not likely to survive the updrafts of convective storms cells. Examination of ~ 2500 ozonesonde-measured ozone profiles at about ~ 20 tropical and mid-latitude ozonesonde stations finds that only 59 profiles have relative humidity greater than 80% over at least 4-km in altitude, not to mention measurements under deep convective cloudy conditions. Studies using mesoscale chemical transport models indicate deep convection can redistribute surface trace gases in the clouds [35–38]. Kley et al. [39] observed near-zero ozone concentration in both the marine boundary layer and the upper troposphere over the convective Pacific, indicating the convective lifting of the ozone-poor surface air to the upper troposphere. Measurements by Strom et al. [40] of the trace gases (i.e., ozone) in two cumulonimbus anvils over western Europe indicated that much of the anvil air is rapidly transported from the surface with limited dilution. Because of the large temporal and spatial variability of surface ozone, the ozone inside the convective clouds may represent larger temporal and spatial variability as well, and its concentration might be larger or smaller than that in the corresponding clear air. Furthermore, the intra-cloud distribution of ozone does not simply follow a redistribution of surface ozone. Photolysis and heterogeneous processes in the clouds [41], chemical reactions specific to thunderstorms [42], and stratospheric intrusion [35,43–46] may lead to production or loss inside the clouds. Dickerson et al. [35], Poulida et al. [44], and Winterrath et al. [46] found enhanced ozone mixing ratios in the mid-latitude convective clouds and ascribed the enhancement to the intrusion of stratospheric air. Winterrath et al. [46] also suggested that the enhanced ozone may be produced by non-lightning discharge mechanisms. Suhre et al. [45] found high concentrations of ozone (100–500 ppbv) in the upper equatorial Atlantic troposphere near strong convective activities contrasting to the near-zero observation in the upper Pacific troposphere by Kley et al. [39]. These very high ozone values were attributed to the downward movement of stratospheric air due to convection or quasi-isentropic transport from the extratropical stratosphere [43,45]. Overall, the limited measurements from case studies and model studies indicate that intra-cloud ozone presents large spatial and temporal variability. Without knowledge of ozone amount and distribution in the clouds, it is impossible to directly estimate the ICOAEN effect by simulating intra-cloud ozone absorption using radiative transfer models.

4.7. Estimation of OREs in tropical convective cloudy areas

Newchurch et al. [4] estimated the cloudy/clear TOC difference after correcting cloud-height errors and incorrect tropospheric climatology at four selected regions in tropical areas. Because the chemical and dynamic effects on cloudy/clear TOC difference are estimated to be small over tropical deep convective cloudy conditions, the remaining cloudy/clear TOC differences can be ascribed

to OREs caused by nonlinearity calibration and the assumption of opaque Lambertian clouds. We use the above process to indirectly estimate the average OREs resulting from assuming opaque Lambertian clouds in the tropical areas (15°S–15°N) during 1979–1983, when the Temperature Humidity Infrared Radiometer cloud data are available. Cloudy pixels with reflectivity $\geqslant 80\%$ and CTP $\leqslant 300$ hPa are selected and pixels with reflectivity $\leqslant 20\%$ are used to represent clear pixels. OREs due to incorrect CTPs are corrected following the procedures described in Newchurch et al. [4]. Clear-sky TOC contains OREs arising from imperfect ozone retrieval efficiency, and the added OZBC contains OREs because the TOMS standard climatology ozone profiles are used instead of actual ozone profiles. The SHADOZ (Southern Hemisphere Additional Ozonesondes) tropospheric ozone profiles [47] are used as actual ozone profiles to correct incorrect tropospheric climatology for both clear and cloudy conditions. In the Southern Hemisphere, this SHADOZ reference is used independent of latitude and interpolated across longitude. The ozone reference in the Northern Hemisphere is the same as that in the Southern Hemisphere but is six months out of phase. From the NIMBUS-7/Earth-Probe TOMS bias in the cloudy/clear TOC difference, about $\sim 4.4 \pm 1.1$ DU is ascribed to OREs caused by nonlinearity calibration that occurs in NIMBUS-7 TOMS data. Finally, we derive the approximate OREs arising from the assumption of opaque Lambertian clouds. The readers are referred to Newchurch et al. [4] for more detail.

Fig. 14 shows the seasonally and annually averaged OREs, which are mainly contributed by the ICOAEN effect for such thick clouds. There is a wave-1 pattern in the errors, usually maximizing over the Atlantic Ocean and Africa and minimizing over the Pacific Ocean. Typically, the ICOAEN effect ranges from 5 to 13 DU over the Atlantic Ocean and Africa, and ranges from 1 to 7 DU over the Pacific Ocean. The wave-1 distribution of OREs is caused by the convective redistribution of surface air. Because of the higher H_2O and lower NO_x marine environment over the Pacific Ocean compared to that over the Atlantic Ocean and Africa, the concentration of surface ozone is lower. The convective redistribution leads to more intra-cloud ozone over the Atlantic Ocean and Africa. Therefore, the ICOAEN effect is larger over the Atlantic Ocean and Africa. The large values of the ICOAEN effect over the North Atlantic Ocean during March–May, with a magnitude of 15–21 DU, might contain significant errors because the approximate actual tropospheric ozone from SHADOZ measurements is shifted by six months in the Northern Hemisphere. The measured monthly mean tropospheric ozone at Paramaribo ($5.8°N, 55.2°W$) [47] during 1999–2001 is about 28.6 DU during March–May, smaller by 14.8 DU than the approximated value over the North Atlantic Ocean. If we use ozone measurements at Paramaribo as the approximate tropospheric ozone for the north Atlantic Ocean, the ICOAEN effect will be reduced by ~ 10 DU to 5–11 DU.

OREs associated with clouds can largely underestimate the derived tropospheric ozone using cloudy/clear difference techniques. The convective-cloudy differential and clear-cloudy pairs methods [48,49] used only cloud fields with monthly minimum OZAC (in the convective-cloudy differential method) or six 5-day minimum OZAC values (in the clear-cloudy pairs method). These cloud fields are closer to tropopause by 30–50 hPa, improving the derived tropospheric ozone only by 2–3 DU. These two methods actually select cloud fields with small OREs or with extremely small OZAC values that partly offset positive OREs, leading to much smaller errors in the derived tropospheric ozone [50]. The use of minimum OZAC values is determined by tuning the derived tropospheric ozone to match the measured tropospheric ozone at selected ozonesonde stations. So large errors can occur in the derived tropospheric ozone at locations other than these ozonesonde stations.

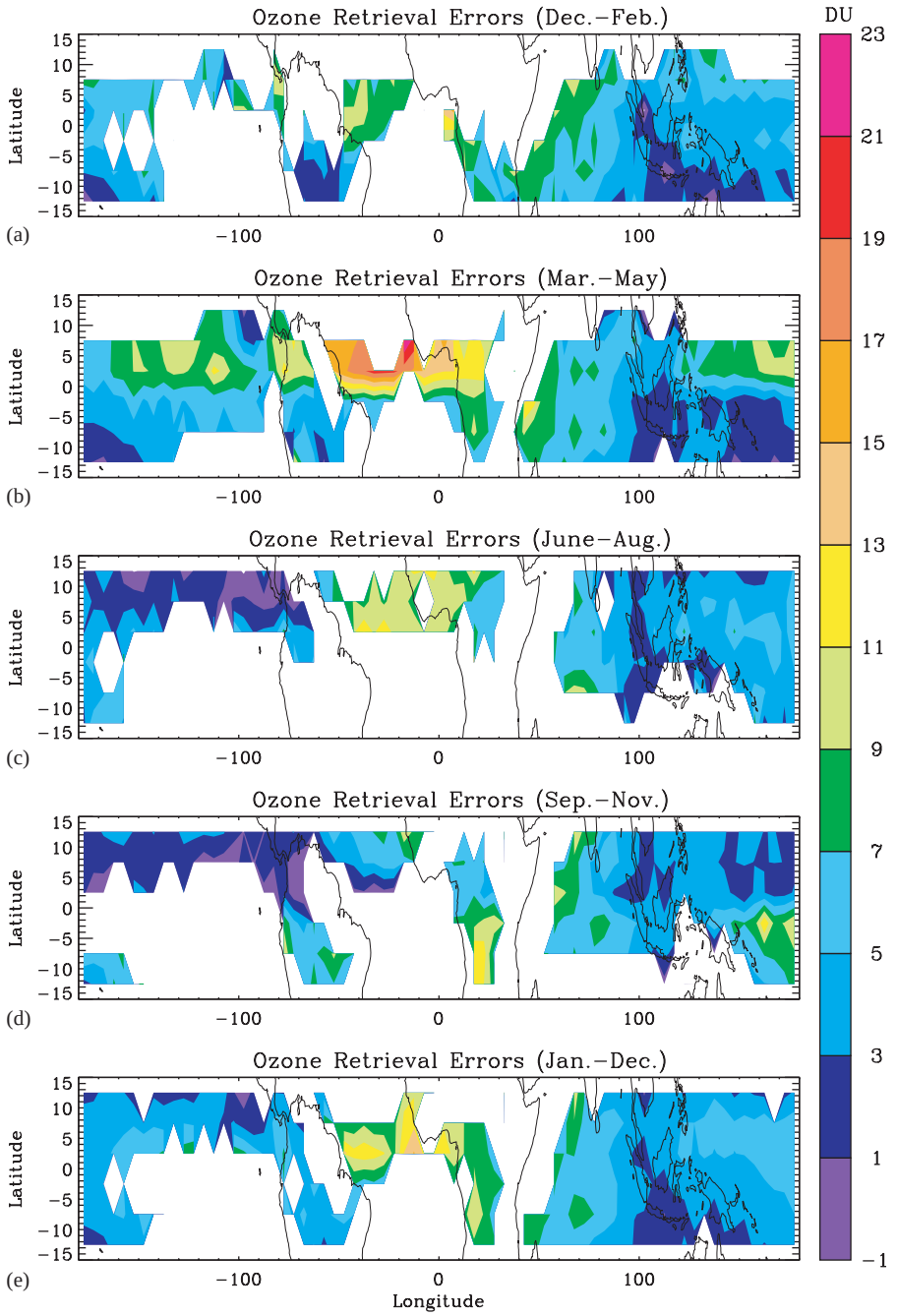

Fig. 14. Ozone retrieval errors for tropical convective clouds (reflectivity $\geqslant 80\%$ and cloud-top pressure $\leqslant 300$ hPa) averaged in 5°-longitude × 5°-latitude areas estimated from TOMS data during 1979–1983. (a)–(d) Seasonally averaged ozone retrieval errors for the winter, spring, summer, and fall, respectively. (e) Annually averaged ozone retrieval errors.

5. Summary and conclusions

The assumption of opaque Lambertian clouds and the employed Partial Cloud Model (PCM) can cause errors in the TOMS retrieved ozone. To simulate measured backscattered radiances, we use a radiative transfer model that treats clouds as scattering media, and then retrieve the total ozone using the TOMS version-7 algorithm. We study ozone retrieval errors (OREs) with different Cloud Optical Properties (COPs), Cloud Optical Depths (CODs), Cloud Geometrical Depths (CGDs), ozone profiles, intra-cloud ozone amounts and distributions, and measurement wavelengths (Earth-Probe vs. NIMBUS-7 TOMS).

The overall OREs are divided into four categories: Lambertian (i.e., assumption of angularly independent Lambertian cloud surfaces), PCM (i.e., the used Partial Cloud Model), ICOAEN (i.e., Intra-Cloud Ozone Absorption ENhancement), and BCOA (i.e., Below-Cloud Ozone Absorption) effects. The Lambertian effect varies with COP, COD, cloud-top height, and ozone profile and results from the air mass factor difference between simulated scattering clouds and assumed Lambertian clouds, profile difference between retrieval and forward calculation, and some slightly nonlinear wavelength dependence in the cloud reflection. But OREs caused by the Lambertian effect are usually within the TOMS retrieval precision at COD $\geqslant 20$, indicating the assumption of angularly independent cloud reflection is fairly good. The PCM effect results primarily from the cloud fraction being underestimated so the added ozone below clouds decreases. At COD $\geqslant 20$, the average PCM effect is within 2.5 DU. The ICOAEN effect occurs because backscattered photons penetrate the clouds and the in-cloud multiple scattering enhances ozone absorption. The ICOAEN effect depends significantly on observation viewing geometry, ozone amount and distribution inside clouds, and CGD. The effective intra-cloud ozone (EICO, i.e., the error) decreases with increasing solar zenith angle and view zenith angle. For homogeneous ozone distribution, the EICO is almost equal to the actual intra-cloud ozone at near nadir view but is close to 0 at larger viewing geometries (e.g., $\theta_0 = 75^\circ$, $\theta = 60^\circ$). The EICO is almost directly proportional to the actual intra-cloud ozone. However, the ratio of effective to actual intra-cloud ozone decreases slightly with increasing actual intra-cloud ozone. The increase of CGD usually increases the amount of actual intra-cloud ozone, therefore increasing the EICO. In the clouds, the sensitivity of the ICOAEN effect to ozone peaks in the upper part of the clouds and decreases dramatically with decreasing altitude below the peak. The ICOAEN effect varies slightly with different COPs; the smaller the asymmetry factor, the smaller the EICO is. Assuming clouds to be ice clouds only slightly decreases the ICOAEN effect. The ICOAEN effect usually decreases with increasing COD, decreasing by 40% when COD increases from 10 to 500. The BCOA effect occurs because backscattered photons penetrate below cloud bottoms and are partly absorbed by ozone. The BCOA effect is significant only when the cloud is optically thin and the amount of ozone below the cloud bottoms is large. The use of TOMS version-7 PCM is good because the negative PCM effect cancels other positive OREs. At smaller CODs (COD $\leqslant 5$), the TOMS version-7 algorithm retrieved approximately the correct ozone because of compensating errors. With increasing CODs, the negative PCM effect decreases more dramatically than other positive effects do. Therefore, the overall OREs are positive and increase with increasing COD until the COD reaches about 20–40, when the PCM effect is very small. Then the overall OREs are dominated by the ICOAEN effect and the further increase of COD slightly decreases the OREs. OREs for forward full clouds apply to forward partial clouds but approximately weighted by forward cloud fractions. Directly correcting OREs caused by assuming opaque Lambertian clouds in TOMS data is impossible because of insufficient knowledge

of cloud parameters and intra-cloud ozone amount and distribution. We estimate from the TOMS cloudy/clear total ozone difference that OREs in the TOMS data are usually 5–13 DU on average over the Atlantic Ocean and Africa and 1–7 DU over the Pacific Ocean for tropical high-altitude and high-reflectivity clouds.

Knowledge of TOMS OREs, especially the ICOAEN effect, applies to ozone/trace gas retrieval from other satellite instruments such as OMI (Ozone Monitoring Instrument), GOME (Global Ozone Monitoring Instrument), and SCIAMACHY (SCanning Imaging Absorption SpectroMeter for Atmospheric ChartographY). Several problems need further study. In this study, we assumed single-layer homogeneous clouds, which clearly is not accurate for clouds of limited horizontal extent and cloud edge pixels. Although this cloud treatment is more realistic than the TOMS treatment, it is still idealized. More detailed work using a 3-D radiative transfer model is needed to study OREs for more realistic clouds such as multi-layer, inhomogeneous, and broken clouds. The current knowledge about how ozone and trace gases are distributed in the clouds is far from sufficient, which is the key to directly correcting ozone retrieval errors. Understanding how trace gases are distributed in convective clouds requires more measurements and further modeling effort using mesoscale transport and chemical models. In addition, the ICOAEN effect indicates that it is possible to derive ozone and other trace gases inside clouds and therefore correct retrieval errors from satellite measurements. O_2–O_2 absorption bands in OMI will provide estimation of photon paths inside clouds and may allow estimation of O_3 and NO_2 inside clouds.

Acknowledgements

We are grateful to the NASA Earth Science Enterprise for supporting this research through the NASA/ACMAP. We wish to thank the Ozone Processing Team at GSFC for providing the TOMS data and processing capability.

References

[1] Rossow WB, Schiffer RA. Advances in understanding clouds from ISCCP. Bull Am Meteorol Soc 1999;80: 2261–87.
[2] Bhartia PK. OMI algorithm theoretical basis document, vol. II: OMI ozone products, 2001.
[3] Chance K. OMI algorithm theoretical basis document, vol. IV: OMI trace gas algorithms, 2001.
[4] Newchurch MJ, Liu X, Kim JH, Bhartia PK. On the accuracy of TOMS retrievals over cloudy regions. J Geophys Res 2001;106:32,315–26.
[5] Knibbe WJJ, de Haan JF, Hovenier JW, Stam DM, Koelemeijer RBA, Stammes P. Deriving terrestrial cloud-top pressure from photopolarimetry of reflected light. JQSRT 2000;64:173–99.
[6] Kurosu T, Rozanov VV, Burrows JP. Parameterization schemes for terrestrial water clouds in the radiative transfer model GOMETRAN. J Geophys Res 1997;102:21,809–23.
[7] Kylling A, Albold A, Seckmeyer G. Transmittance of a cloud is wavelength-dependent in the UV-range: physical interpretation. Geophys Res Lett 1997;24:397–400.
[8] Mayer B, Kylling A, Madronich S, Seckmeyer G. Enhanced absorption of UV radiation due to multiple scattering in clouds: experimental evidence and theoretical explanation. J Geophys Res 1998;103:31,241–54.
[9] Erle F, Pfeilsticker K, Platt U. On the influence of tropospheric clouds on zenith-scattered-light measurements on stratospheric species. Geophys Res Lett 1995;22:2725–8.
[10] Brewer AW, Kerr JB. Total ozone measurements in cloudy weather. Pure Appl Geophys 1973;106–108:929–37.

[11] Dobson GMB, Normand CWB. Determination of constants used in the calculation of the amount of ozone from spectrophotometer measurements and an analysis of the accuracy of the results. Ann Int Geophys Yr 1962;XVI: 161–91.
[12] Fioletov VE, Kerr JB, Wardle DI. The relationship between total ozone and spectral UV irradiance from Brewer observations and its use for derivation of total ozone form UV measurements. Geophys Res Lett 1997;24: 2997–3000.
[13] Fischer J, Grassl H. Detection of cloud-top height from backscattered radiances within the oxygen-A band—part I: theoretical study. J Appl Meteorol 1991;30:1245–59.
[14] Saiedy F, Jacobowitz H, Wark DQ. On cloud-top determination from Gemini-5. J Atmos Sci 1965;24:63–9.
[15] Wu MC. Remote sensing of cloud-top pressure using reflected solar radiation in the oxygen-A band. J Clim Appl Meteorol 1985;24:539–46.
[16] McPeters RD, Bhartia PK, Krueger AJ, Herman JR, Schlesinger BM, Wellemeyer CG, Seftor CJ, Jaross G, Taylor SL, Swissler T, Torres O, Labow G, Byerly W, Cebula RP. NIMBUS-7 Total Ozone Mapping Spectrometer (TOMS) data products user's guide. NASA Reference Publication 1996.
[17] Koelemeijer RBA, Stammes P. Effects of clouds on ozone column retrieval from GOME UV measurements. J Geophys Res 1999;104:8281–94.
[18] Herman BM, Caudill TR, Flittner DE, Thome KJ, Ben-David A. Comparison of the Gauss-Seidel spherical polarized radiative transfer code with other radiative transfer codes. Appl Opt 1995;34:4563–72.
[19] Bass AM, Paur RJ. The ultraviolet cross-sections of ozone, I: the measurements. In: Zerefos CS, Ghazi A, editors. Atmospheric ozone. Massachusetts: Reidel D, 1984. p. 606–10.
[20] Paur RJ, Bass AM. The ultraviolet cross-sections of ozone, II: Results and temperature dependence. In: Zerefos CS, Ghazi A, editors. Atmospheric ozone. Massachusetts: Reidel D, 1984. p. 611–6.
[21] Bates DR. Rayleigh scattering by air. Planet Space Sci 1984;32:785–99.
[22] Macke A, Muller J, Raschke E. Single scattering properties of atmospheric ice crystals. J Atmos Sci 1996;53: 2813–25.
[23] Hale GM, Querry MR. Optical constants of water in the 200-nm to 200-m wavelength region. Appl Opt 1973;12: 555–63.
[24] Han Q, Rossow WB, Lacis AA. Near-global survey of effective droplet radii in liquid water clouds using ISCCP data. J Clim 1994;7:465–97.
[25] Mishchenko MI, Dlugach JM, Yanovitskij EG, Zakharova NT. Bidirectional reflectance of flat, optically thick particulate layers: an efficient radiative transfer solution and applications to snow and soil surfaces. JQSRT 1999;63:409–32.
[26] Mishchenko MI, Rossow WB, Macke A, Lacis AA. Sensitivity of cirrus cloud albedo, bidirectional reflectance, and optical thickness retrieval accuracy to ice particle shape. J Geophys Res 1996;101:16,973–85.
[27] Rossow WB, Schiffer RA. ISCCP cloud data products. Bull Am Meteorol Soc 1991;72:2–20.
[28] Rossow WB, Walker AW, Beuschel DE, Roiter MD. International Satellite Cloud Climatology Project (ISCCP) documentation of new cloud dataset. Geneva: WMO/TD; 1996. p. 737.
[29] Bohren CF, Huffman DH. Absorption and scattering of light by small particles. New York: Wiley; 1983. p. 530.
[30] Warren SG. Optical constants of ice from ultraviolet to the microwave. Appl Opt 1984;23:1205–25.
[31] Doutriaux-Boucher M, Buriez J, Brogniez G, C-Labonnote L, Baran AJ. Sensitivity of retrieved POLDER directional cloud optical thickness to various ice particle models. Geophys Res Lett 2000;27:109–12.
[32] Twomey S, Jacobowitz H, Howell HB. Light scattering by cloud layers. J Atmos Sci 1967;24:70–9.
[33] Hudson RD, Kim JH, Thompson AM. On the derivation of tropospheric column ozone from radiances measured by the total ozone mapping spectrometer. J Geophys Res 1995;100:11,137–45.
[34] Klenk KF, Bhartia PK, Fleig AJ, Kaveeshwar VG, McPeters RD, Smith PM. Total ozone determination from the backscattered ultraviolet (BUV) experiment. J Appl Meteorol 1982;21:1672–84.
[35] Dickerson RR, Huffman GJ, Luke WT, Nunnermacker LJ, Pikering KE, Leslie ACD, Lindsey CG, Slinn WGN, Kelly TJ, Daum PH, Delany AC, Greenberg JP, Zimmerman PR, Boatman JF, Ray JD, Stedman DH. Thunderstorms: an important mechanism in the transport of air pollutants. Science 1987;235:460–5.
[36] Pickering KE, Thompson AM, Dickerson RR, Luke WT, McNamara DP, Greenberg JP, Zimmerman PR. Model calculations of tropospheric ozone production potential following observed convective events. J Geophys Res 1990;95:14,049–62.

[37] Pickering KE, Thompson AM, Scala JR, Tao WK, Simpson J, Garstang M. Photochemical ozone production in tropical squall line convection during NASA global tropospheric experiment/Amazon boundary layer experiment 2A. J Geophys Res 1991;96:3099–114.
[38] Pickering KE, Thompson AM, Tao WK, Kucsera TL. Upper tropospheric ozone production following mesoscale convection during STEarth-Probe/EMEX. J Geophys Res 1993;98:8737–49.
[39] Kley D, Crutzen PJ, Smit HGJ, Vomel H, Oltmans SJ, Grassl H, Ramanathan V. Observations of near-zero ozone concentrations over the convective Pacific: effects on air chemistry. Science 1996;274:230–3.
[40] Strom J, Fischer H, Lelieveld J, Schroder F. In-situ measurements of microphysical properties and trace gases in two cumulonimbus anvils over Western Europe. J Geophys Res 1999;104:12,221–6.
[41] Lelieveld J, Crutzen PJ. Influences of cloud photochemical processes on tropospheric ozone. Nature 1990;343: 227–33.
[42] Ridley BA, Walega JG, Dye JE, Grahek FE. Distributions of NO, NO_x, NO_y, and O_3 to 12 km altitude during the summer monsoon season over New Mexico. J Geophys Res 1994;99:25,519–34.
[43] Crutzen PJ, Lawrence M. Ozone clouds over the Atlantic. Nature 1997;388:625–6.
[44] Poulida O, Dickerson RR, Heymsfield A. Stratosphere-troposphere exchange in a mid-latitude mesoscale convective complex, 1: observations. J Geophys Res 1996;101:6823–36.
[45] Suhre K, Cammas JP, Nedelec P, Rosset R, Marenco A, Smit HGJ. Ozone-rich transients in the upper equatorial Atlantic troposphere. Nature 1997;388:661–3.
[46] Winterrath T, Kurosu TP, Richter A, Burrows JP. Enhanced O_3 and NO_2 in thunderstorm clouds: Convection or production? Geophys Res Lett 1999;26:1291–4.
[47] Thompson AM, Oltmans SJ, Schmidlin FJ, Logan JA, Fujiwara M, Kirchhoff VWJH, Posny F, Coetzee GJR, Hoegger B, Kawakami S, Ogawa T, Johnson BJ, Vömel H, Labow G. The 1998–2000 SHADOZ (Southern Hemisphere Additional Ozonesondes) tropical ozone climatology. 1: Comparison with TOMS and ground-based measurements. J Geophys Res 2003;108:10.1029/2001JD000967.
[48] Ziemke JR, Chandra S, Bhartia PK. Two new methods for deriving tropospheric column ozone from TOMS measurements: assimilated UARS MLS/HALOE and convective-cloud differential techniques. J Geophys Res 1998;103:22,115–27.
[49] Newchurch MJ, Sun D, Kim JH, Liu X. Tropical tropospheric ozone derived using Clear-Cloudy Pairs (CCP) of TOMS measurements. Atmos Chem Phys Discuss 2002;3:225–52.
[50] Liu X. Ozone retrieval errors associated with clouds in Total Ozone Mapping Spectrometer (TOMS) data. PhD dissertation 2002. University of Alabama in Huntsville, Huntsville.